Topological quantum quench dynamics carrying arbitrary Hopf and second Chern numbers

Motohiko Ezawa

Phys. Rev. B **98**, 205406 — Published 9 November 2018

DOI: 10.1103/PhysRevB.98.205406

Topological quantum quench dynamics carrying arbitrary Hopf and second-Chern numbers

Motohiko Ezawa
Department of Applied Physics, University of Tokyo, Hongo 7-3-1, 113-8656, Japan

A quantum quench is a nonequilibrium dynamics governed by the unitary evolution. We propose a two-band model whose quench dynamics is characterized by an arbitrary Hopf number belonging to the homotopy group $\pi_3(S^2) = \mathbb{Z}$. When we quench a system from an insulator with the Chern number $C_i \in \pi_2(S^2) = \mathbb{Z}$ to another insulator with the Chern number C_f, the preimage of the Hamiltonian vector forms links having the Hopf number $C_f - C_i$. We also investigate a quantum-quench dynamics for a four-band model carrying an arbitrary second-Chern number $N \in \pi_4(S^4) = \mathbb{Z}$, which can be realized by quenching a three-dimensional topological insulator having the three-dimensional winding number $N \in \pi_3(S^3) = \mathbb{Z}$.

I. INTRODUCTION:

Topological physics has been investigated intensively in this decade. It is characterized by a topological number quantized for distinct phases. Topological properties are extensively studied in equilibrium, while they are yet to be explored in nonequilibrium. One successful example is a Floquet system[1–6], where the external field is oscillating. Quantum quench is another method to create a nonequilibrium state, where some parameters are suddenly changed, and afterwards the wave function develops under unitary transformation[7–12].

The Hopf number is described by the homotopy class $\pi_3(S^2)$, which is a linking number in three dimensions. It is naturally realized in a two-band system in physical system, since it is characterized by S^2. Nontrivial Hopf textures are discussed for cold atoms[13,14], light fields[15] and liquid crystal[16]. The topological Hopf insulator is a three-dimensional (3D) topological insulator possessing a nonzero Hopf number[17–22]. The topological Hopf semimetal has been proposed, whose Fermi surface contains linked loop nodes[23–27]. Recently, the Hopf number also appears in the 2D topological insulator after quench[25,28–32]. It is shown that the Hopf number is 1 when the system turns from a trivial insulator to a topological insulator with the Chern number 1. This topological quantum quench has already been realized in cold atoms by performing quasimomentum-resolved Bloch-state tomography for the azimuthal phase[33–35]. There are several studies on the quench from a trivial insulator to a topological insulators, while there are few studies on the quench from a topological insulator to a trivial insulator or the quench from a topological insulator to another topological insulator.

The second-Chern number was originally introduced in the context of the time-reversal invariant topological insulators in three dimension[36], which is constructed by the dimensional reduction of 4D topological insulators characterized by the second-Chern number. Since the second-Chern number is characterized by the homotopy $\pi_4(S^4)$, it requires 4D space. However, in quantum quench dynamics, since time introduces an additional dimension, the second-Chern number can be defined in 4D space-time. Indeed, a quantum quench carrying the second-Chern number was recently proposed[32], where the system is quenched from a trivial insulator to a topological insulator indexed by the 3D winding number $\pi_3(S^3)$.

In this paper, we propose a model which is characterized by an arbitrary Hopf number after quench. For this purpose, we first construct a model carrying an arbitrary Chern number on square lattice. The dynamics of the density matrix is analytically solved in this system. We show that the Hopf number is identical to the difference of the Chern numbers between the initial and final phases. Finally, we propose a quantum quench dynamics carrying arbitrary second-Chern numbers.

II. MODEL

We consider a two-band tight-binding model defined on square lattice. The Hamiltonian is given by

$$H = \begin{pmatrix} F_1 & F_2 \\ F_2^* & -F_1 \end{pmatrix}, \tag{1}$$

where

$$F_1 = t_1 (\cos k_x + \cos k_y) + t_2 \cos k_x \cos k_y - m, \tag{2}$$

$$F_2 = (\sin k_x + i \sin k_y)^N \tag{3}$$

in momentum space, with N being an integer. It has Dirac cones at the Γ point $(k_x, k_y) = (0, 0)$, the M point (π, π), the X point $(\pi, 0)$ and the Y point $(0, \pi)$. The mass is given by the diagonal element F_1 at the Dirac point, which reads

$$M_\Gamma = 2t_1 + t_2 - m \tag{4}$$

at the Γ point,

$$M_M = -2t_1 + t_2 - m \tag{5}$$

at the M point, and

$$M_X = M_Y = -t_2 - m \tag{6}$$

at the X and Y points.

There are several topological phases in the Hamiltonian. The topological phase diagram is constructed by examining the Dirac masses. The phase boundaries are determined by the condions $M_\Gamma = M_M = M_X = M_Y = 0$ as in Fig.2.

The Hamiltonian is rewritten as

$$H = \boldsymbol{d} \cdot \boldsymbol{\sigma} \tag{7}$$

in terms of the Pauli matrices $\boldsymbol{\sigma}$. The normalized vector $\hat{\boldsymbol{d}} = \boldsymbol{d}/|\boldsymbol{d}|$ points a Bloch sphere and thus forms an S^2 manifold. Hence, the Chern number is defined to characterize the

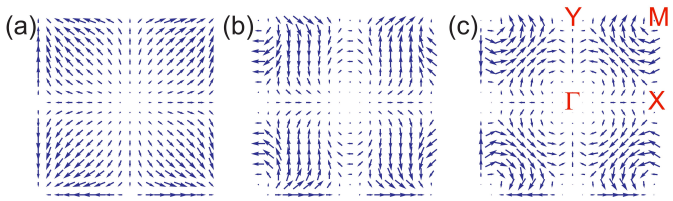

FIG. 1: Hamiltonian vector with (a) $N = 1$, (b) $N = 2$ and (c) $N = 3$. They form meron structure with the winding number N at the high-symmetry points Γ, M, X and Y,

Hamiltonian, which is the Pontryagin number,

$$C = -\frac{1}{4\pi}\int_{\mathrm{BZ}} d^2k[\hat{\boldsymbol{d}}\cdot(\partial_{k_x}\hat{\boldsymbol{d}}\times\partial_{k_y}\hat{\boldsymbol{d}})]. \tag{8}$$

We show the $\boldsymbol{d}$ vector in Fig.1. It exhibits meron structures at the Γ, M, X and Y points. In the vicinity of the high-symmetry points $K = \Gamma, M, X$ and Y, since $F_1 = M_K$, we may approximate the Hamiltonian as

$$H_K = \begin{pmatrix} M_K & k^N_{+\xi} \\ k^N_{-\xi} & -M_K \end{pmatrix}, \tag{9}$$

where we have defined $k_\pm = k_x \pm ik_y$ and $\xi = +$ for the Γ and M points and $\xi = -$ for the X and Y points. The $\boldsymbol{d}$ vector winds N times around the z axis as the azimuthal angle increases from 0 to 2π. The total Chern number is thus given by

$$\begin{aligned} C &= \sum_K \xi\frac{N}{2}\mathrm{sgn}\left(M_K\right) \\ &= \frac{N}{2}\mathrm{sgn}\left(2t_1+t_2-m\right)+\frac{N}{2}\mathrm{sgn}\left(-2t_1+t_2-m\right) \\ &\quad + N\mathrm{sgn}\left(t_2+m\right). \end{aligned} \tag{10}$$

We show the topological phase diagram in Fig.2. It has five phases indexed by the Chern numbers $C = 0, \pm N, \pm 2N$.

III. QUANTUM QUENCH

We investigate a quantum quench of the Hamiltonian beween two phases in the phase diagram in Fig.2. We start with an initial Hamiltonian where $\boldsymbol{d} = \boldsymbol{d}^i$. At a certain time t_0, we suddenly change it to the final Hamiltonian where $\boldsymbol{d} = \boldsymbol{d}^f$, while keeping the system to remain in the ground state of the initial Hamiltonian. (We choose $t_0 = 0$ for simplicity.) After the quantum quench, the system is no longer the ground state but an excited state with respect to the final Hamiltonian. For $t > t_0$, the dynamics is described by the density matrix $\rho_\pm = |\psi_\pm\rangle\langle\psi_\pm|$ satisfying the Liouville-von-Neumann equation,

$$i\frac{\partial\rho_\pm(k,t)}{\partial t} = \left[H^f(k),\rho_\pm(k,t)\right], \tag{11}$$

whose solution is given by an unitary evolution as

$$\rho_\pm(k,t) = e^{-iH^f(k)t}\rho_\pm(k,0)\,e^{iH^f(k)t}. \tag{12}$$

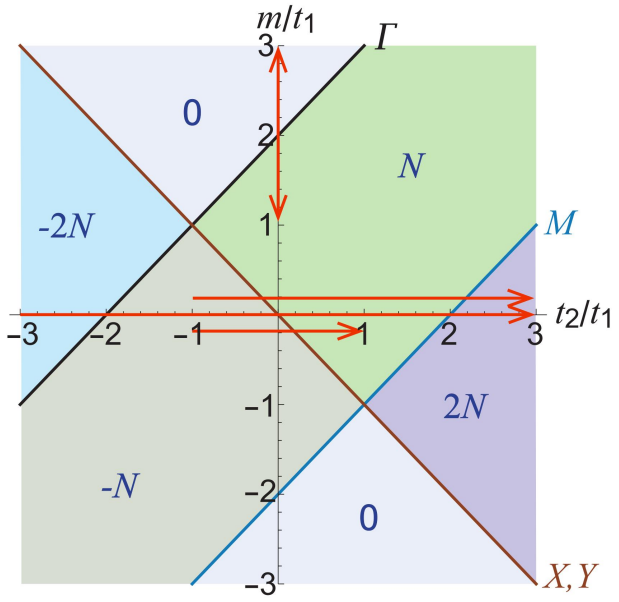

FIG. 2: Topological phase diagram as a function of t_2/t_1 and m/t_1. The Chern number is shown in each phase. The phase boundaries are determined by the condition $M_K = 0$, where K stands for the high-symmetry point indicated in the figure. The arrows in red represent the quantum quench processes we have numerically studied.

In the two-band system, the density matrix is rewritten in terms of the $\boldsymbol{d}$ vector as

$$\rho_\pm(k,0) = \left[1\pm\hat{\boldsymbol{d}}^i\cdot\boldsymbol{\sigma}\right]/2. \tag{13}$$

The time-evolved density matrix is then given by[30]

$$\rho_\pm(k,t) = \left[1\pm\hat{\boldsymbol{d}}(k,t)\cdot\boldsymbol{\sigma}\right]/2, \tag{14}$$

with the time-evolved $\boldsymbol{d}$ vector

$$\hat{\boldsymbol{d}}(k,t) = \boldsymbol{e}_1 + \boldsymbol{e}_2\cos(2\varepsilon t) + \boldsymbol{e}_3\sin(2\varepsilon t), \tag{15}$$

where we have defined an orthogonal basis[30]

$$\boldsymbol{e}_1 = \hat{\boldsymbol{d}}^f\left(\hat{\boldsymbol{d}}^i\cdot\hat{\boldsymbol{d}}^f\right), \tag{16}$$

$$\boldsymbol{e}_2 = \hat{\boldsymbol{d}}^i - \hat{\boldsymbol{d}}^f\left(\hat{\boldsymbol{d}}^i\cdot\hat{\boldsymbol{d}}^f\right), \tag{17}$$

$$\boldsymbol{e}_3 = \hat{\boldsymbol{d}}^i\times\hat{\boldsymbol{d}}^f. \tag{18}$$

The $\boldsymbol{d}$ vector is initially $\boldsymbol{d}^i$ and rotates on the Bloch sphere with period π/ε. Hereafter, we rescale the time as $\tau = \varepsilon t$. Then, the quench dynamics is periodic with period π as a function of τ, forming a manifold S^1. The mapping from (k_x, k_y, τ) to the Bloch sphere is a mapping from the T^3 to the S^2, which is characterized by the Hopf number.

We study various quantum quench processes from an insulator with C_i to another insulator with C_f. We first study a quantum quench from a trivial insulator to a topological insulator, and then a quantum quench from a topological insulator to a trivial insulator, and finally a quantum quench from a topological insulator to another topological insulator

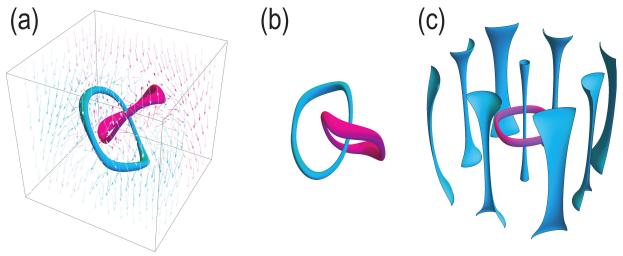

FIG. 3: Trivial to topological quench. Bird's eye's view of the almost zero-energy surface of the Hamiltonian vector with $N = 1$. They form closed linking structures. We have quenched from the trivial state with the mass $m/t_1 = 3$ to the topological state with the mass $m/t_1 = 1$ while keeping $t_2/t_1 = 0$ to draw figures. (a) The preimage of $\hat{d}_y = 1$ is colored in magenta, while that of $\hat{d}_y = -1$ is colored in cyan. (b) The preimage of $\hat{d}_x = 1$ is colored in magenta, while that of $\hat{d}_x = -1$ is colored in cyan. (c) The preimage of $\hat{d}_z = 1$ is colored in magenta, while that of $\hat{d}_z = -1$ is colored in cyan. The $\boldsymbol{d}$ vectors are also shown in (a).

IV. TRIVIAL TO TOPOLOGICAL QUENCH

First, we consider a quantum quench from a trivial insulator to a topological insulator with N. We show the d vector in Fig.3(a), where the preimages of $\hat{d}_y(k_x, k_y, \tau) = \pm 1$ in the space time (k_x, k_y, τ) are also shown. We also show the preimages of $\hat{d}_x(k_x, k_y, \tau) = \pm 1$ and $\hat{d}_z(k_x, k_y, \tau) = \pm 1$ in Fig.3(b) and (c), respectively. All of them have the identical linking number. Hence it is enough to show only one of them. In the following we only show the preimages of $\hat{d}_y(k_x, k_y, \tau) = \pm 1$. In Fig.4, we find the two preimages form torus links with the Hopf number N. We numerically calculate the quench dynamics between the trivial insulator with $m/t_1 = 3$ and the topological insulator with $m/t_1 = 1$ while keeping $t_2/t_1 = 0$. See the vertical arrow in the phase diagram (Fig.2), where the vertical arrow crosses only the phase boundary determined by $M_\Gamma = 0$.

It is possible to construct an analytical expression for a quantum quench from a trivial insulator with the mass $m = \infty$ to a topological insulator with the mass M_Γ. Note that the trivial insulators with $m/t_1 = 3$ and $m = \infty$ belong to the same phase. In this quench, since the sign of the mass M_Γ is relevant, it is enough to analyze the low-energy theory in the vicinity of the Γ point, where the wave function of the Hamiltonian (9) is given by

$$|\psi(t=0)\rangle = \frac{1}{c}\begin{pmatrix} \left(M_\Gamma + \sqrt{k^{2N} + M_\Gamma^2}\right) k_{+\xi}^N \\ 1 \end{pmatrix} \tag{19}$$

with c the normalization constant. Hence, the initial wave function is $|\psi(t=0)\rangle = (1,0)^t$ for $m = \infty$. By using

$$e^{-iH^f\tau} = \begin{pmatrix} \cos\tau - i\hat{d}_z \sin\tau & -i\hat{d}_- \sin\tau \\ -i\hat{d}_+ \sin\tau & \cos\tau + i\hat{d}_z \sin\tau \end{pmatrix}, \tag{20}$$

the time-evolved wave function is expressed as

$$|\psi(\tau)\rangle = e^{-iH^f\tau}|\psi(0)\rangle = \begin{pmatrix} \cos\tau - i\hat{d}_z \sin\tau \\ -i\hat{d}_+ \sin\tau \end{pmatrix}. \tag{21}$$

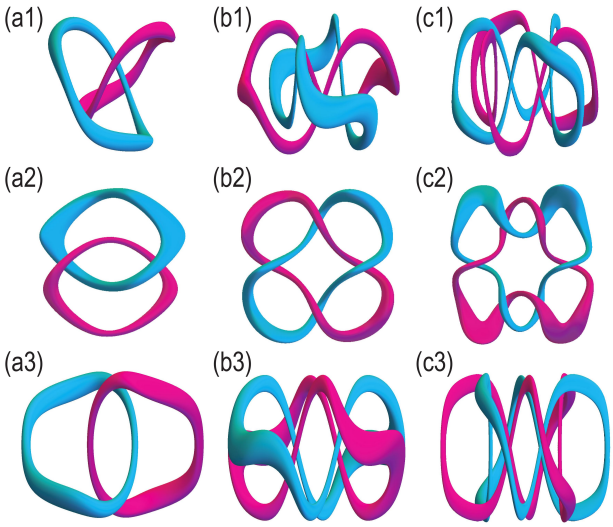

FIG. 4: Trivial to topological quench. Bird's eye's view of the almost zero-energy surface of the Hamiltonian vector with (a1) $N = 1$, (b1) $N = 2$ and (c1) $N = 3$. They form closed linked loops. We have quenched from the trivial state with the mass $m/t_1 = 3$ to the topological state with the mass $m/t_1 = 1$ while keeping $t_2/t_1 = 0$ to draw figures. The preimage of $\hat{d}_y = 1$ is colored in magenta, while that of $\hat{d}_y = -1$ is colored in cyan. (a2)–(c2) and (a3)–(c3) are the corresponding top and side views.

Making a cylindrical symmetric parametrization,

$$\hat{d}_+ = \frac{k_{+\xi}^N}{k^N}\sin\theta(k), \qquad \hat{d}_z = \cos\theta(k), \tag{22}$$

with

$$\cos\theta(k) = \frac{M_\Gamma}{\sqrt{k^{2N} + M_\Gamma^2}}, \quad \sin\theta(k) = \frac{k^N}{\sqrt{k^{2N} + M_\Gamma^2}}, \tag{23}$$

we obtain the Berry connection

$$A_x = \sin\tau\sin\theta(k)\left[-\frac{Nk_y}{k^2}\sin\tau\sin\theta(k) + \frac{k_x}{k}\theta'(k)\cos\tau\right], \tag{24}$$

$$A_y = \sin\tau\sin\theta(k)\left[\frac{Nk_x}{k^2}\sin\tau\sin\theta(k) + \frac{k_y}{k}\theta'(k)\cos\tau\right], \tag{25}$$

$$A_t = -\cos\theta(k), \tag{26}$$

and the Berry curvature

$$F_x = 2\sin\tau\sin\theta(k)\left[-\frac{Nk_x}{k}\cos\tau\sin\theta(k) + \frac{k_y}{k}\partial_k\theta(k)\sin\tau\right], \tag{27}$$

$$F_y = -2\sin\tau\sin\theta(k)\left[\frac{Nk_y}{k}\cos\tau\sin\theta(k) + \frac{k_x}{k}\partial_k\theta(k)\sin\tau\right], \tag{28}$$

$$F_t = \frac{N}{k}\partial_k\theta(k)\sin^2\tau\sin 2\theta(k). \tag{29}$$

By using

$$\boldsymbol{A}\cdot\boldsymbol{F} = -\frac{2N}{k}\left[\partial_k\cos\theta(k)\right]\sin^2\tau, \tag{30}$$

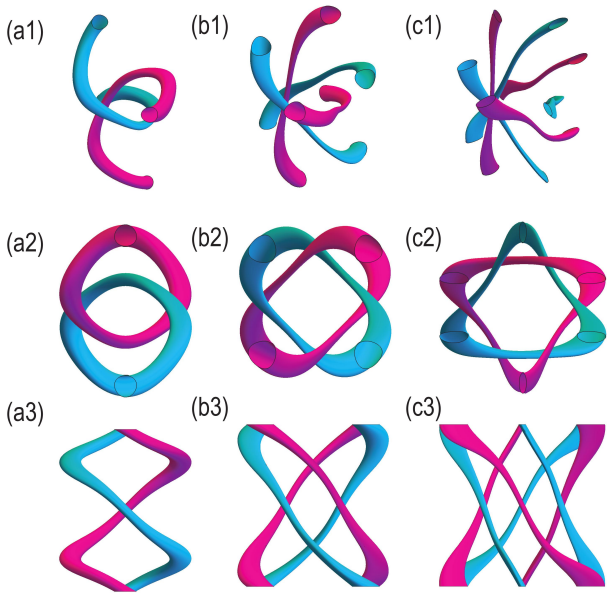

FIG. 5: Topological to trivial quench. Bird's eye's view of the almost zero-energy surface of the Hamiltonian vector with (a1) $N=1$, (b1) $N=2$ and (c1) $N=3$. They form open linked helix. We have quenched from the topological states with the mass $m/t_1=1$ to the trivial states with the mass $m/t_1=3$ while keeping $t_2/t_1=0$ to draw figures. The preimage of $\hat{d}_y=1$ is colored in magenta, while that of $\hat{d}_y=-1$ is colored in cyan. (a2)–(c2) and (a3)–(c3) are the corresponding top and side views.

the Hopf number is calculated as

$$\begin{aligned}\chi &= \frac{1}{\pi}\int_0^{\pi} d\tau \int_0^{\infty} kdk \boldsymbol{A}\cdot\boldsymbol{F} \\ &= -N\left[\lim_{k\to\infty}\cos\theta\left(k\right)-\cos\theta\left(0\right)\right] \\ &= -N\left[\lim_{k\to\infty}\frac{M_\Gamma}{\sqrt{k^{2N}+M_\Gamma^2}}-\mathrm{sgn}M_\Gamma\right] \\ &= N\mathrm{sgn}M_\Gamma. \end{aligned} \tag{31}$$

It is identical to the change of the Chern number at the Γ point since the Chern number at the Γ point is given by $\frac{N}{2}\mathrm{sgn}M_\Gamma$. Namely, the Hopf number is identical to the Chern number C_f.

V. TOPOLOGICAL TO TRIVIAL QUENCH

We next consider a quantum quench from a topological insulator with N to a trivial insulator. We show the preimages of $\hat{d}_y\left(k_x,k_y,\tau\right)=\pm1$ in Fig.5, where the two preimages form open helix links with the Hopf number N. We numerically calculate the quench dynamics between the topological insulator with $m/t_1=1$ and the trivial insulator with $m/t_1=3$ while keeping $t_2/t_1=0$: See the vertical arrow in the phase diagram (Fig.2).

It is possible to analytically discuss the Hopf number in an extreme case of the quantum quench from a topological insulator with the mass M_Γ to a trivial insulator with the infinite mass $m=\infty$. By inserting the final state $\hat{\boldsymbol{d}}^f=(0,0,-1)$ into (15) and we find

$$\boldsymbol{e}_1=\left(0,0,d_z^i\right),\quad \boldsymbol{e}_2=\left(d_x^i,d_y^i,0\right),\quad \boldsymbol{e}_3=\left(d_y^i,-d_x^i,0\right), \tag{32}$$

and

$$\begin{aligned}\hat{\boldsymbol{d}}\left(k,\tau\right)=&\left(\cos\left(2\varepsilon t\right)d_x^i+\sin\left(2\varepsilon t\right)d_y^i,\right.\\ &\left.\cos\left(2\varepsilon t\right)d_y^i-\sin\left(2\varepsilon t\right)d_x^i,d_z^i\right).\end{aligned} \tag{33}$$

The time-evolved Hamiltonian is proportional to

$$\hat{\boldsymbol{d}}\left(k,\tau\right)\cdot\boldsymbol{\sigma}=\begin{pmatrix}\hat{d}_z & \hat{d}_-e^{2i\tau}\\ \hat{d}_+e^{-2i\tau} & -\hat{d}_z\end{pmatrix}. \tag{34}$$

In the vicinity of the Γ point, the wave function is given by

$$\left|\psi\left(\tau\right)\right\rangle=\frac{1}{c}\begin{pmatrix}-e^{2i\tau}\left(-M_\Gamma+\sqrt{k^{2N}+M_\Gamma^2}\right)\\ k_+^N\end{pmatrix}. \tag{35}$$

The Berry connection is given by

$$A_x=-\frac{Nk_y}{2k^2}\left(2+\frac{M_\Gamma}{\sqrt{k^{2N}+M_\Gamma^2}}\right), \tag{36}$$

$$A_y=\frac{Nk_x}{2k^2}\left(2+\frac{M_\Gamma}{\sqrt{k^{2N}+M_\Gamma^2}}\right), \tag{37}$$

$$A_t=1-\frac{M_\Gamma}{\sqrt{k^{2N}+M_\Gamma^2}}, \tag{38}$$

and the Berry curvature is given by

$$F_x=\frac{NM_\Gamma k_y}{k^{2N-2}\left(k^{2N}+M_\Gamma^2\right)^{3/2}}, \tag{39}$$

$$F_y=-\frac{NM_\Gamma k_x}{k^{2N-2}\left(k^{2N}+M_\Gamma^2\right)^{3/2}}, \tag{40}$$

$$F_t=\frac{N^2M_\Gamma}{k^{2N-2}\left(k^{2N}+M_\Gamma^2\right)^{3/2}}. \tag{41}$$

By using

$$\boldsymbol{A}\cdot\boldsymbol{F}=-\frac{N^2M_\Gamma}{k^{2N-2}\left(k^{2N}+M_\Gamma^2\right)^{3/2}}, \tag{42}$$

the Hopf number is calculated as

$$\begin{aligned}\chi &= \frac{1}{\pi}\int_0^{\pi} d\tau \int_0^{\infty} kdk \boldsymbol{A}\cdot\boldsymbol{F} \\ &= -\int_0^{\infty}\frac{N^2M_\Gamma}{k^{2N-2}\left(k^{2N}+M_\Gamma^2\right)^{3/2}}kdk \\ &= -N\mathrm{sgn}M_\Gamma. \end{aligned} \tag{43}$$

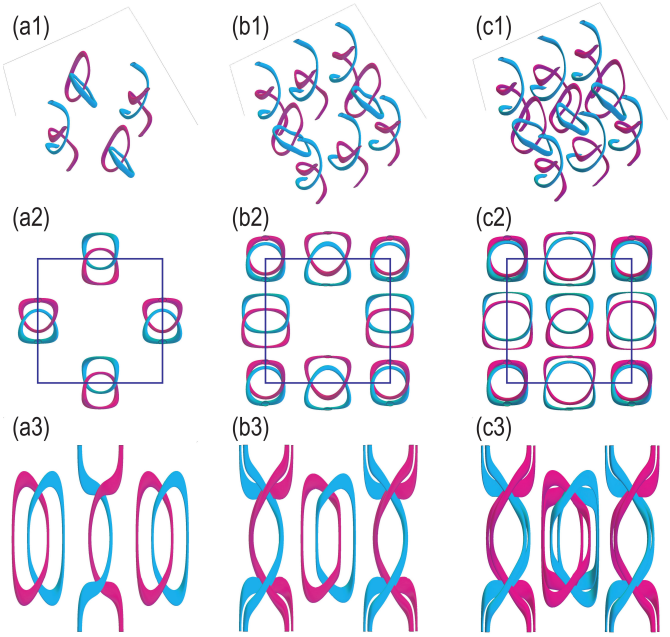

FIG. 6: Topological to topological quench (a) from a topological insulator with $C_i = -1$ to another topological insulator with $C_f = 1$, (b) from a topological insulator with $C_i = -1$ to another topological insulator with $C_f = 2$ and (c) from a topological insulator with $C_i = -2$ to another topological insulator with $C_f = 2$. The Brillouin zone is indicated by the square. The preimage of $\hat{d}_y = 1$ is colored in magenta, while that of $\hat{d}_y = -1$ is colored in cyan.

As a result, we find the Hopf number to be N. We note that the signs of (31) and (43) are opposite since the two processes are the inverse processes. As in the case of the trivial to topological quench, it is identical to the change of the Chern number at the Γ point since the Chern number at the Γ point is given by $\frac{N}{2}\mathrm{sgn}M_\Gamma$. Namely, the Hopf number is identical to the Chern number $-C_i$.

VI. TOPOLOGICAL TO TOPOLOGICAL QUENCH

Finally, we study quench from a topological insulator to another topological insulator. We show preimages in Fig.6 for the case of $N = 1$. We find that torus links and open helix links with the Hopf number N appear at the high-symmetry points where the sign of the mass changes and the Hopf number is identical to $C_f - C_i$. We explicitly study the following three cases, where the parameter t_2 is quenched while keeping $m = 0$: See the horizontal arrows in the phase diagram given in Fig.2. In the following, we study the case with $N = 1$ for simplicity, where links with the Hopf number 1 emerge at the high-symmetry points.

(a) For example, if we quench from the topological insulator with $t_2/t_1 = -1$ and $C_i = -1$ to the topological insulator with $t_2/t_1 = 1$ and $C_f = 1$, two Hopf links with the Hopf number 1 appear at the X and Y points since the sign of the masses at the X and Y points change [Fig.6(a)]. Then the total Hopf number is 2, which is identical to the difference of the Chern numbers. The shape of the Hopf link at the X point is the closed loop, while that at the Y point is the open helix. It seems that the C_4 symmetry is violated. However, this is an artifact due to the preimages of $\hat{d}_y = \pm 1$. The closed loop and the open helix are inverted when we plot the preimages of $\hat{d}_x = \pm 1$.

(b) When we quench from the topological insulator with $t_2/t_1 = -1$ and $C_i = -1$ to the topological insulator with $t_2/t_1 = 3$ with $C_f = 2$, three Hopf links with the Hopf number 1 appear at the X, Y and M points [Fig.6(b)]. Then the total Hopf number is 3.

(c) In the same way, when we quench from the topological insulator with $t_2/t_1 = -3$ and $C_i = -2$ to the topological insulator with $t_2/t_1 = 3$ with $C_f = 2$, three Hopf links with the Hopf number 1 appear at the Γ, X, Y and M points [Fig.6(c)]. Then the total Hopf number is 4.

VII. QUANTUM QUENCH WITH SECOND-CHERN NUMBER

A quantum quench carrying the second-Chern number 1 has been proposed[32]. We generalize it to a quantum quench carrying an arbitrary second-Chern number N.

We consider the Hamiltonian

$$H = \sum_{\alpha=x,y,z} f_\alpha(\boldsymbol{k})\tau_x\sigma_\alpha + m(\boldsymbol{k})\tau_z\sigma_0, \tag{44}$$

where τ and σ represent the Pauli matrices, while σ_0 is the unit matrix. We define a unit vector

$$d_{\boldsymbol{k}} = \frac{1}{|E(\boldsymbol{k})|}(f_x(\boldsymbol{k}), f_y(\boldsymbol{k}), f_z(\boldsymbol{k}), m(\boldsymbol{k})) \tag{45}$$

with the energy

$$E(\boldsymbol{k}) = \pm\sqrt{\sum_{\alpha=x,y,z} f_\alpha^2(\boldsymbol{k}) + m^2(\boldsymbol{k})}. \tag{46}$$

Since the unit vector forms a three sphere S^3, the Hamiltonian is characterized by the 3D winding number[37,38] ν_3 describing the third Homotopy $\pi_3(S^3) = \mathbb{Z}$,

$$\nu_3 = \frac{1}{2\pi^2}\int_{\mathrm{BZ}} d^3k\varepsilon^{abcd}\hat{d}_a\partial_{k_x}\hat{d}_b\partial_{k_y}\hat{d}_c\partial_{k_z}\hat{d}_d. \tag{47}$$

The unitary evolution is given by $U(t) = \exp[-i\tau H]$. When we start with the initial state $|\psi(0)\rangle = (1,0,0,0)^t$, the quenched wave function is given by

$$\begin{aligned}|\psi(\tau)\rangle &= e^{-iH^f\tau}|\psi(0)\rangle \\ &= (\cos\tau, -im_{\boldsymbol{k}}\sin\tau, 0, \\ &\quad -if_{z,\boldsymbol{k}}\sin\tau, (f_{y,\boldsymbol{k}} - if_{x,\boldsymbol{k}})\sin\tau)^t.\end{aligned} \tag{48}$$

We define the order parameter as

$$\boldsymbol{L} = \langle\psi_{\boldsymbol{k}}(t)|(\tau_x\sigma_x, \tau_x\sigma_y, \tau_x\sigma_z, \tau_z, \tau_y)|\psi_{\boldsymbol{k}}(t)\rangle, \tag{49}$$

which forms the four sphere S^4 since $\boldsymbol{L}$ is a unit vector satisfying $|\boldsymbol{L}| = 1$. It is classified by the fourth homotopy $\pi_4(S^4)$, where the dynamical second-Chern number is defined by[32,36]

$$C_2 = -\frac{3}{8\pi^2}\int_0^{\pi/2} dt \int_{\rm BZ} d^3k \varepsilon^{abcde} L_a \partial_{k_x} L_b \partial_{k_y} L_c \partial_{k_z} L_d \partial_t L_e. \tag{50}$$

It is shown that the dynamical second-Chern number is identical to the 3D winding number[32]

$$C_2 = \nu_3 \frac{3}{4\pi^2}\int_0^{\pi/2} \sin^3 2\tau d\tau = \nu_3 \tag{51}$$

with (47).

Now we explicitly study the model given by

$$f_x(\boldsymbol{k}) = {\rm Re}[(\sin k_x + i \sin k_y)^N], \tag{52}$$
$$f_y(\boldsymbol{k}) = {\rm Im}[(\sin k_x + i \sin k_y)^N], \tag{53}$$
$$f_z(\boldsymbol{k}) = \sin k_z, \tag{54}$$
$$m(\boldsymbol{k}) = m - t_1(\cos k_x + \cos k_y + \cos k_z). \tag{55}$$

It follows that the 3D winding number is given by $\nu_3 = N$ for $1 < |m/t_1| < 3$, $\nu_3 = -2N$ for $|m/t_1| < 1$ and $\nu_3 = 0$ for $|m/t_1| > 3$. Accordingly, the quantum quench is characterized by the second-Chern number N.

VIII. CONCLUSION

We have constructed models of quantum quench, which are characterized by an arbitrary Hopf number or by an arbitrary second-Chern number. We have explored new types of topological quantum quenches. One is the topological to trivial quench and the other is the topological to topological quench, which have different link structures compared to the previously studied trivial to topological quench.

The author is very much grateful to N. Nagaosa for many helpful discussions on the subject. This work is supported by the Grants-in-Aid for Scientific Research from MEXT KAKENHI (Grant No. JP18H03676, No.JP17K05490, and No.15H05854). This work is also supported by CREST, JST (JPMJCR16F1).

[1] T. Oka and H. Aoki, Phys. Rev. B **79**, 081406(R) (2009).
[2] T. Kitagawa, T. Oka, A. Brataas, L. Fu, and E. Demler, Phys. Rev. B **84**, 235108 (2011).
[3] N. Lindner, G. Refael and V. Gaslitski, Nat. Phys. **7**, 490 (2011).
[4] B. Dóra, J. Cayssol, F. Simon and R. Moessner, Phys. Rev. Lett. **108**, 056602 (2012).
[5] M. Ezawa, Phys. Rev. Lett. **110**, 026603 (2013).
[6] N. Goldman and J. Dalibard, Phys. Rev. X **4**, 031027 (2014).
[7] M. D. Caio, N. R. Cooper, and M. J. Bhaseen, Phys. Rev. Lett. **115**, 236403 (2015)
[8] Y. Hu, P. Zoller, and J. C. Budich, Phys. Rev. Lett. **117**, 126803 (2016).
[9] L. Zhang, L. Zhang, and X.-J. Liu, cond-mat/arXiv:1807.10782
[10] S.-F. Liou and K. Yang, Phys. Rev. B 97, 235144 (2018)
[11] X. Qiu, T.-S. Deng, G.-C. Guo and W. Yi, Phys. Rev. A 98, 021601(R) (2018)
[12] Z. Gong and M. Ueda, cond-mat/arXiv:1710.05289
[13] Y. Kawaguchi, M. Nitta, and M. Ueda, Phys. Rev. Lett. **100**, 180403 (2008).
[14] D. S. Hall, M. W. Ray, K. Tiurev, E. Ruokokoski, A. H. Gheorghe and M. Mottonen, Nat. Phys. **12**, 478 (2016).
[15] H. Kedia, I. Bialynicki-Birula, D. Peralta-Salas, and W. T. M. Irvine, Phys. Rev. Lett. **111**, 150404 (2013).
[16] P. J. Ackerman and I. I. Smalyukh, Phys. Rev. X **7**, 011006 (2017).
[17] J. E. Moore, Y. Ran and X.-G. Wen, Phys. Rev. Lett. **101**, 186805 (2008).
[18] D.-L. Deng, S.-T. Wang, and L.-M. Duan, Phys. Rev. B **89**, 075126 (2014).
[19] D.-L. Deng, S.-T. Wang, C. Shen, and L.-M. Duan, Phys. Rev. B **88**, 201105(R) (2013).
[20] D.-L. Deng, S.-T. Wang, K. Sun, and L.-M. Duan, Chinese Physics Letters, **35**, 1 (2018)
[21] R. Kennedy, Phys. Rev. B **94**, 035137 (2016).
[22] C. Liu, F. Vafa and C. Xu, Phys. Rev. B **95**, 161116 (2017).
[23] W. Chen, H.-Z. Lu, and J.-M. Hou, Phys. Rev. B **96**, 041102 (2017).
[24] Z. Yan, R. Bi, H. Shen, L. Lu, S.-C. Zhang, and Z. Wang, Phys. Rev. B **96**, 041103(R) (2017).
[25] P.-Y. Chang and C.-H. Yee, Phys. Rev. B **96**, 081114 (2017).
[26] M. Ezawa, Phys. Rev. B **96**, 041202(R) (2017)
[27] G. Chang, S.-Y. Xu, X. Zhou, S.-M. Huang, B. Singh, B. Wang, I. Belopolski, J. Yin, S. Zhang, A. Bansil, H. Lin, M. Z. Hasan, Phys. Rev. Lett. 119, 156401 (2017)
[28] C. Wang, P. Zhang, X. Chen, J. Yu, and H. Zhai, Phys. Rev. Lett. **118**, 185701 (2017).
[29] M. Tarnowski, F. Nur Unal, N. Flaschner, B. S. Rem, A. Eckardt, K. Sengstock, C. Weitenberg, cond-mat/arXiv:1709.01046
[30] C. Yang, L. Li, S. Chen, Phys. Rev. B **97**, 060304 (2018)
[31] J. Yu, cond-mat/arXiv:1804.10358
[32] P.-Y Chang, Phys. Rev. B **97**, 224304 (2018)
[33] N.Flaschner, B.Rem, M.Tarnowski, D.Vogel, D.-S.Luhmann, K. Sengstock, and C. Weitenberg, Science **352**, 1091 (2016).
[34] N. Flaschner, D. Vogel, M. Tarnowski, B. S. Rem, D. S. Luhmann, M. Heyl, J. C. Budich, L. Mathey, K. Sengstock, and C. Weitenberg, Nat. Phys. **14**, 265 (2018)
[35] P. Hauke, M. Lewenstein, and A. Eckardt, Phys. Rev. Lett. **113**, 045303 (2014)
[36] X.-L. Qi, T. L. Hughes, S.-C. Zhang, Phys. Rev. B **78**, 195424 (2008)
[37] A. P. Schnyder, S. Ryu, A. Furusaki, A. W. W. Ludwig, Phys. Rev. B **78**, 195125 (2008)
[38] G.E. Volovik, JETP Lett. **90**, 587, (2009)